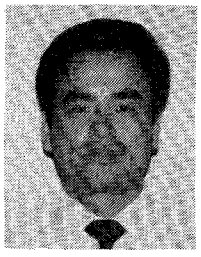

Eiji Hagihara was born in Yokkaichi, Japan, in 1950. He received the B.S. and M.S. degrees in applied physics from Nagoya University, Nagaya, Japan, in 1973 and 1975, respectively.

He joined Yokosuka Electrical Communication Laboratory, Japan, in 1975, and has been engaged in the research of millimeter-wave solid-state circuits and millimeter-wave integrated circuits. He is now a Manager at the Kinki Telecommunication Bureau, Nippon Telegraph and Telephone Public Corporation, Osaka, Japan.

Mr. Hagihara is a member of the Institute of Electronics and Communication Engineers of Japan.

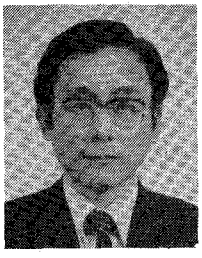

Masami Akaike was born in Kamakura-shi, Kanagawa-ken, Japan, on October 15, 1940. He received the B.S., M.S., and Ph.D. degrees from the University of Tokyo, Tokyo, Japan, in 1964, 1966, and 1969, respectively.

He joined the Musashino Electrical Communication Laboratory, Nippon Telegraph and Telephone Public Corporation, Tokyo, Japan, in 1969. He was engaged in the research of millimeter-wave solid-state circuits and the development and design of repeaters and measuring equipments for a guided millimeter-wave transmission system. He is currently a Chief of the INS Model Development Division, Musashino Electrical Communication Laboratory, NTT.

Dr. Akaike is a member of the Institute of Electronics and Communication Engineers of Japan, and was a recipient of the 1971 IECEJ Yonezawa Memorial Scholarship.

Kazuyuki Yamamoto was born in Kyoto, Japan, on July 13, 1946. He received the B.S., M.S., and Ph.D. degrees in electrical engineering, from the University of Kyoto, Japan, in 1969, 1971, and 1982, respectively.

Since joining the Electrical Communication Laboratory, Nippon Telegraph and Telephone Public Corporation, Tokyo, Japan, in 1971, he has been engaged in the research and development of filters, solid-state circuits, and transmission lines for millimeter and submillimeter wavelength regions. He is currently a Staff Engineer of the Radio Transmission Section, Integrated Transmission System Development Division, Yokosuka Electrical Communication Laboratory, NTT.

Mr. Yamamoto is a member of the Institute of Electronics and Communication Engineers of Japan.

Broad-Band Characteristics of EHF IMPATT Diodes

LOWELL H. HOLWAY, JR. AND SHIOU LUNG CHU

Abstract—**Measurements have been made of the oscillator characteristics when a GaAs EHF double-drift IMPATT diode designed for a frequency of 35 GHz is operated over an extended frequency range from 33–50 GHz. The diode which was designed for 35 GHz has a broad-band capability which allows it to produce 2.15 W at 44.1 GHz. An analytic model is shown to predict accurately the observed results. The model indicates that the upper limit in frequency can be increased by reducing the diode area or the series resistance as well as by reducing the length of the drift region.**

I. Introduction

THE BROAD-BAND characteristics of IMPATT diodes make them a flexible power source for use in many applications. In this paper we describe a theoretical and experimental study of the power output of a GaAs double-drift diode designed for 35 GHz when it is operated over an extended frequency range from 33–50 GHz.

The diode was operated in a top-hat circuit in which the circuit parameters were varied in order to optimize the output power at a given frequency and dc-current level. The experimental results are compared with calculations based on an analytic model described previously [1]–[4]. This analytic model uses the Read equation to describe the time behavior of the avalanche zone and assumes that the saturation current is small, that ionization in the drift region is negligible, and that the carriers move at saturated velocities. One of the important parameters of the model is the series resistance. In these calculations, we use values measured accurately by a method described elsewhere [5]. The calculated results of the model were then in close agreement with the experimental results. This model allows

Manuscript received April 7, 1982; revised June 21, 1982.

The authors are with the Raytheon Research Division, 131 Spring Street, Lexington, MA 02173.

0018-9480/82/1100-1933$00.75 ©1982 IEEE

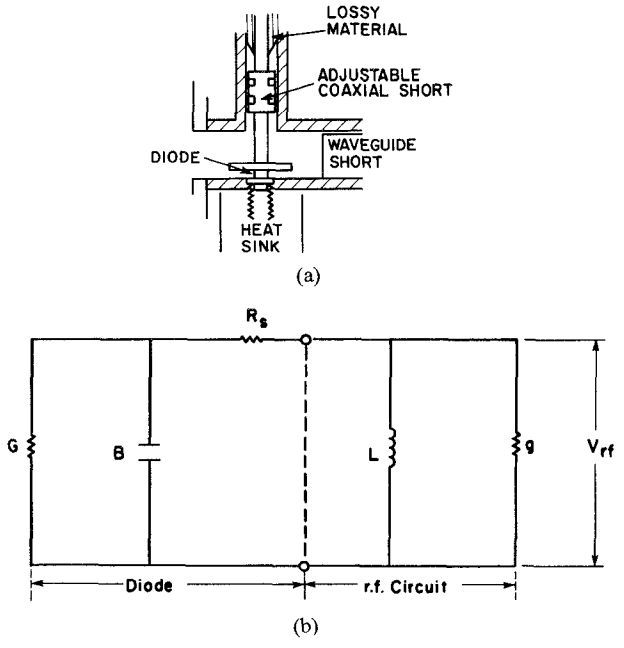

Fig. 1. (a) Sketch of "top-hat" configuration with sliding short. (b) Lumped element equivalent RF circuit for the diode and the external circuit.

us to draw useful conclusions as to the relative importance of different parameters such as drift length, junction area, and series resistance in determining the frequency response of an IMPATT diode.

Diodes were tested with both copper and diamond heat sinks. With the diamond heat sink, a diode designed for 35 GHz produced 2.15W with 14.4-percent efficiency at 44.1 GHz.

II. Experimental Technique

The RF tests were made in a circuit similar to the top-hat circuit described by Misawa [6]. The RF test cavity used in our tests is sketched in Fig. 1. With a given value of the dc current, the circuit was adjusted carefully to obtain the maximum possible output power consistent with the requirement that the oscillation occurred at a specified frequency. Over a small frequency range, one can represent the device operation by the lumped circuit model shown in Fig. 1(b). Here G and B are the conductance and susceptance of the IMPATT diode, R_s is the series resistance, L is the load inductance which is adjusted to maintain the desired frequency, and g is the load conductance.

In one type of measurement, the circuit is tuned to maintain a specified frequency while I_{dc}, the dc current through the diode, is slowly increased. At successive current levels, the tuning is adjusted to give the maximum output power. In terms of the lumped element equivalent circuit of Fig. 1(b), we can picture the load conductance g being adjusted to give the maximum power while the inductance L is changed as necessary to maintain the specified frequency. The output power is

$$P_{out} = \frac{1}{2} g V_{rf}^2 \tag{1}$$

while an oscillation can only occur if V_{rf} can adjust itself to satisfy the condition

$$g = -G - B^2 R_s. \tag{2}$$

Equation (2) is valid in the limit where BR_s and GR_s are both small compared to unity. In this limit the V_{rf} across the diode is nearly the same as the V_{rf} across the load.

III. The Analytical Model

The analytical model for small saturation current, which has been described earlier [2]–[4], is reproduced in the Appendix. For the double-drift GaAs diode used in these experiments, it is an excellent approximation to assume that the drift regions are symmetric. Hereafter, in this paper we assume $v_n = v_p$ and $w_n = w_p$ to reduce the algebra, although there is no difficulty in carrying through a more general calculation.

A. Conditions Near the Oscillation Threshold

At low current levels, where $\omega_R^2/\omega^2 \ll 1$, an explicit expression can be obtained for the RF voltage and the optimum load conductance. These expressions are used for illustrating the oscillation process, but at higher currents where the approximation is invalid, we will use a numerical solution for the admittance in (A1).

When $\omega_R^2/\omega^2 \ll 1$, the real part of (A1) simplifies to

$$G = -2\frac{(1-\cos\theta)}{\theta}\frac{I_{dc}}{V_{rf}}\frac{I_1(b)}{I_0(b)} \tag{3}$$

where $\theta = \omega w_n/v_n = \omega w_p/v_p$ is the common transit angle and

$$b = \frac{3\alpha' v_s}{\omega w_T} V_{rf}. \tag{4}$$

Near the oscillation threshold, b is small which allows the modified Bessel functions in (3) to be expanded in a power series, giving

$$G = -\frac{3\alpha'}{2\theta^2}(1-\cos\theta) I_{dc}\left(1 - \frac{9}{32}\frac{\alpha'^2}{\theta^2} V_{rf}^2\right) \tag{5}$$

where terms proportional to V_{rf}^4 and higher powers are neglected.

Oscillation can only occur when the negative conductance exceeds B^2R_s in magnitude, which requires I_{dc} to exceed a threshold value, given by (5) as

$$I_{th} = \frac{2\theta^2\omega^2 C_d^2 R_s}{3\alpha'(1-\cos\theta)}. \tag{6}$$

Now, as the dc current increases above the threshold, we continually adjust the load conductance to give the maximum output power, which means that

$$\frac{\partial P_{out}}{\partial g} = 0 \tag{7}$$

where P_{out} is given by (1). Solving (7) and (2) when $\Delta I = I_{dc} - I_{th}$ is small compared with I_{th} gives

$$g = \frac{3\alpha'}{4\theta^2}(1-\cos\theta)\Delta I \tag{8}$$

and

$$V_{rf}^2 = \frac{16\theta^2}{9\alpha'^2}\frac{\Delta I}{I_{th}} \tag{9}$$

where we have neglected terms proportional to ΔI^2. Thus, when ΔI is small, the output power increases as

$$P_{out} = \frac{2(1-\cos\theta)}{3\alpha'}\frac{\Delta I^2}{I_{th}}. \tag{10}$$

The power output for the case in which g is adjusted to maximize the power output can be compared with the case where g is kept small but constant as the current is increased. Then V_{rf}^2 increases at exactly twice the rate given by (9) while the output power increases linearly with ΔI, as has been shown elsewhere [5]. A numerical solution for V_{rf} near the threshold current is plotted in Fig. 2 as a dashed curve for g fixed at 0.051 mS and as a solid curve when g is continually adjusted to optimize the output power. The dotted curve in Fig. 2 is the parabola defined by (9); it can be seen that this approximate formula is virtually identical with the numerical calculation. The threshold calculations were all made for the diode 33637, No. 48, which was assumed to be operating at 35.7 GHz and 50°C. The results are in agreement with experimental measurements for $g = 0.051$ mS, described elsewhere [5].

B. Operation at Higher Current Levels

At higher current levels where the threshold approximation loses accuracy, numerical solutions of the analytic model will be used. Moreover, Fig. 2 shows the RF voltage becoming larger as the current increases, while it is usually assumed that the RF voltage cannot become larger than about one-half the dc voltage [7]. For X-band devices, it has already been observed [2] that the measured conductance agrees closely with the conductance calculated from the analytic model for small V_{rf}, except that the measured conductance falls rapidly below the predicted conductance when V_{rf} exceeds a critical value which we call V_{rfmax}. Similarly, the measured conductance for an EHF diode was found to drop abruptly when V_{rf} exceeded a V_{rfmax} equal to 11 V, as shown in Fig. 3(a), for measurements taken at 200°C with a 200-mA dc current.

As described elsewhere [2]–[4], these G versus V_{rf} curves are generated by first calibrating the "top-hat" circuit S-parameters using the known capacitance and series resistance of the chip biased below breakdown and then using these S-parameters to calculate G from the measured reflection coefficients when the diode is generating microwave power.

The electric field profile for the diode in Fig. 3(a) at room-temperature breakdown is shown in Fig. 3(b), based on a computer reconstruction using data at various etch depths measured by a CV digital profilometer. The measurements described below were on wafer 33637 which has a profile similar to Fig. 3(b). Therefore, we will assume that at 200°C, the diodes from this wafer will also have V_{rfmax} equal to 11 V. Adlerstein and Moore [4] found good agreement with experimental measurements when they assumed that V_{rfmax} scaled with temperature in proportion to the measured variation of the breakdown voltage. At 200°C, the breakdown voltage is 19.4 V so that a V_{rfmax} of 11 V is 57 percent of the breakdown voltage, which is comparable

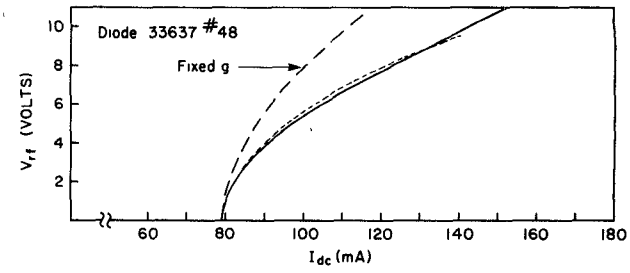

Fig. 2. Calculated RF voltage versus current near threshold conditions. Dashed curve: fixed $g = 0.051$ mS; solid curve: g varied to maximize output power; dotted curve: threshold approximation. $f = 35.7$ GHz.

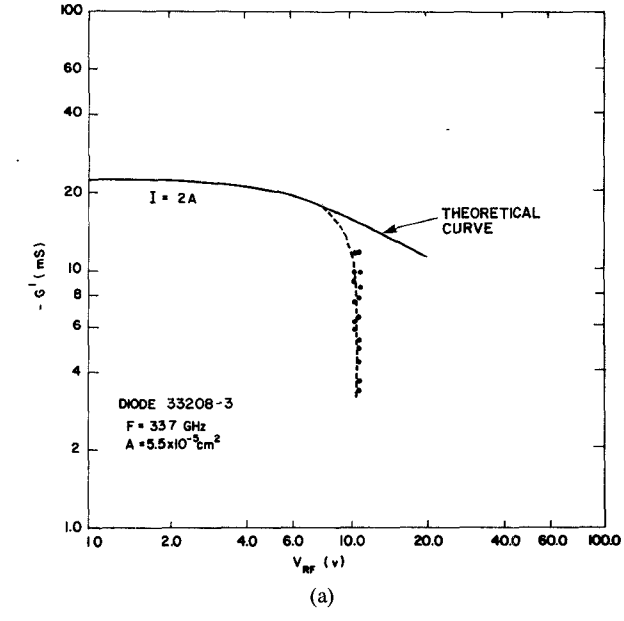

(a)

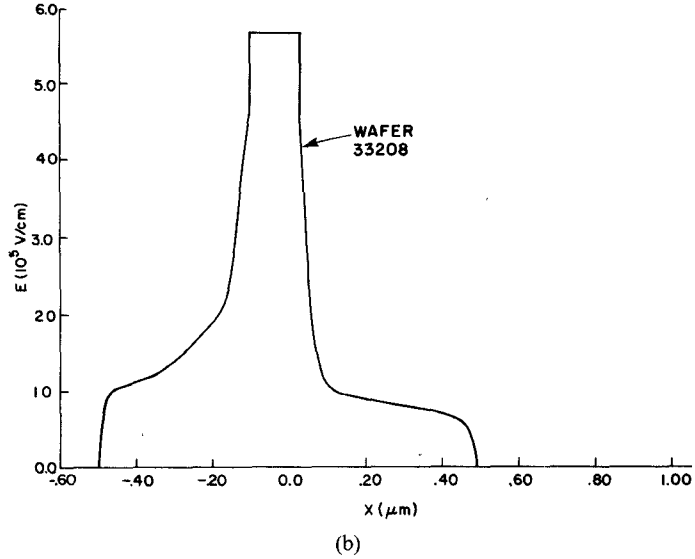

(b)

Fig. 3. (a) Negative conductance versus RF voltage. The measured points (·) are compared to theoretical calculations. (b) Electric field profile at room temperature breakdown based on computerized reconstruction from CV data.

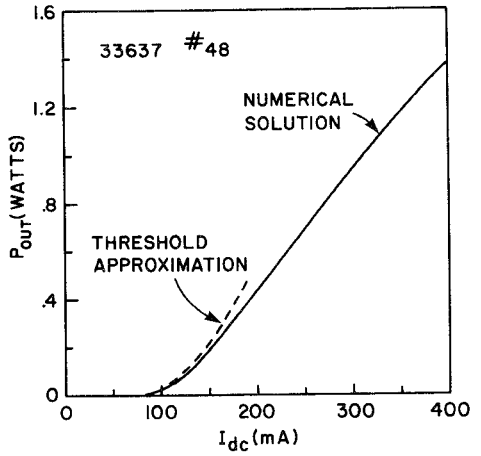

Fig. 4. Calculated output power versus current. $f = 35.7$ GHz, $T = 50°C$. $V_{rf} = V_{rfmax} = 11$ V for I_{dc} above 152 mA.

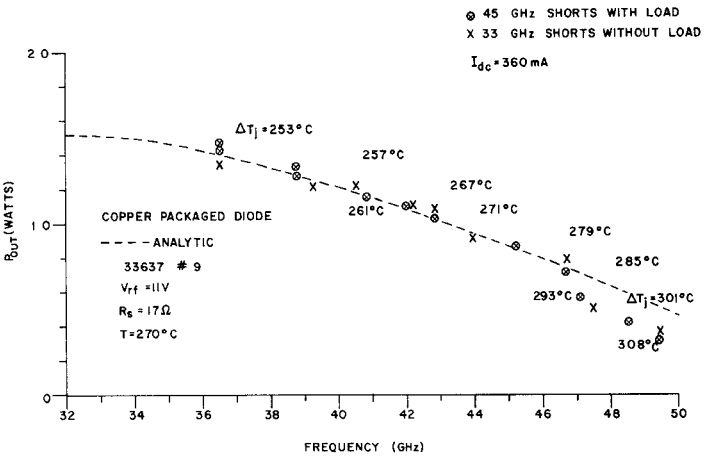

Fig. 5. Measured and calculated output power versus frequency for diode 33637, no. 9. ΔT_j is listed for the experimental points. Dashed curve: numerical calculation assuming $V_{rfmax} = 11$ V and $T = 270°C$.

to the ratio of 50 percent that Read originally suggested [7].

According to the numerical results plotted in Fig. 2, V_{rf} increases rapidly as the current is increased above the threshold value and approaches 11 V near 152 mA. In Fig. 4, the solid curve shows the results of a numerical solution of the analytical model when g is varied to optimize the power output while V_{rf} is constrained to be less than 11 V. The dashed curve in Fig. 4, which was calculated from the threshold approximation of (10), is close to the numerical result until the dc current exceeds 200 mA.

IV. Measurements of Output Power Versus Frequency

Measurements of maximum output power versus frequency for a fixed dc current were made on the two diodes listed in Table I. The values of R_s given in the table were measured by the threshold method [5]. For each of these experiments, the expected maximum power was calculated by a numerical solution of the analytic model assuming $V_{rfmax} = 11$ V. The physical characteristics used in calculations for wafer 33637 are given in Table II. The velocities and ionization coefficients were based on measurements in [8] and [9]. Although the values in Table II are given for 200°C, they were changed appropriately when calculations were made at other temperatures.

The measurements for the device 33637, No. 9 are shown in Fig. 5. The device has a copper heat sink so that at 360 mA the diode is thermally limited, as indicated by the values of ΔT_j shown in the figure. The calculations, which assumed a diode temperature of 270°C, agree closely with the experiment. In making these comparisons it is assumed that the top-hat circuit has 100-percent efficiency.

Similar measurements were taken on wafer 33637, No. 48, as shown in Fig. 6. Because this diode had a diamond heat sink, the dc current could be increased to 500 mA while maintaining satisfactory values of ΔT_j. This device had a series resistance of 0.39 Ω compared with 0.17 Ω for the copper heat sink, so that it produced less power when operated at the same dc current. For example, at 360 mA, the output at 44 GHz dropped from 0.94 W to 0.82 W.

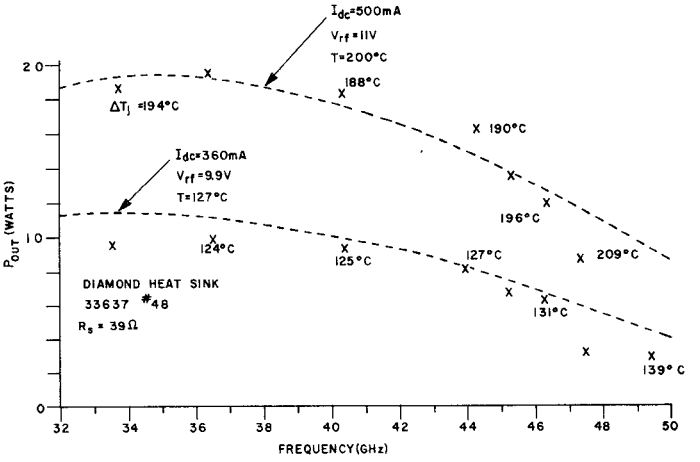

Fig. 6. Measured and calculated output power versus frequency for diode 33637, no. 48. (X) Experimental points. The dashed curves are calculated for 500 mA ($V_{rf} = 11$ V, $T = 200°C$) and for 360 mA ($V_{rf} = 9.9$ V, $T = 127°C$). ΔT_j is listed for the experimental points.

TABLE I
Measured Device Characteristics

Diode	A (10^{-5} cm^2)	θ (°C/W)	R_s (Ω)
33637 No. 9	7.04	34.9	0.17
33637 No. 48	6.14	18.8	0.39

TABLE II
Physical Characteristics of Wafer 33637 at 200°C

$w_n = w_p = 0.48$ μm
$w_a = 0.18$ μm
$E_{AV} = 5.8 \times 10^5$ V/cm
$v_n = v_p = 4.7 \times 10^6$ cm/sec
$\alpha = 5.6 \times 10^4$ cm^{-1}
$\alpha' = 0.225$ V^{-1}

However, at 500 mA the diamond package produced 1.5 W with a ΔT_j of only 190°C.

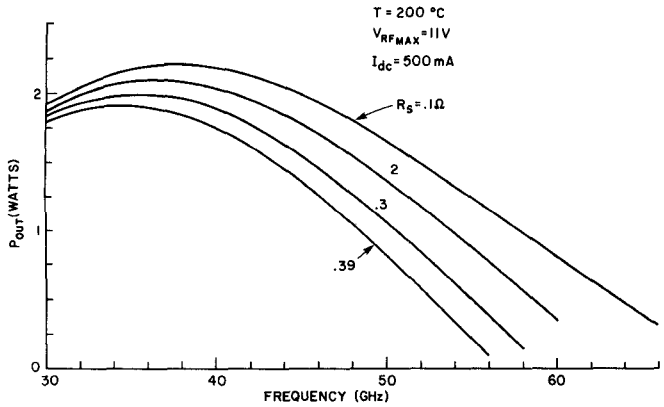

Fig. 7. Calculated output power versus frequency. The calculations of Fig. 6 for 500 mA are modified by assuming the series resistance is reduced to the indicated values.

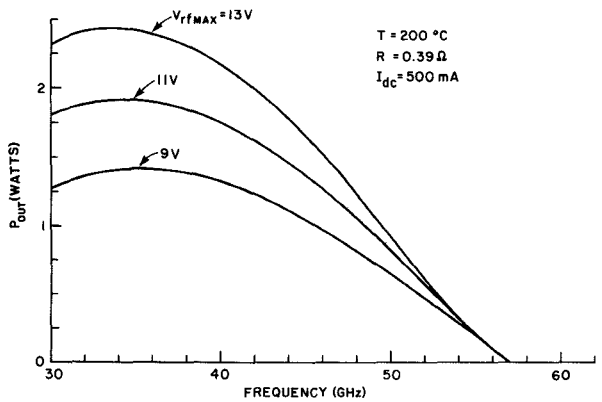

Fig. 8. Calculated output power versus frequency. The calculations of Fig. 6 for 500 mA are modified by assuming V_{rfmax} is changed to the indicated values.

For the numerical calculation, V_{rfmax} was kept at 11 V for the 500-mA case but, assuming it decreases in proportion to the breakdown voltage at lower temperatures, it was taken to be 9.9 V for the 360-mA curve. The material characteristics were evaluated at 200°C for 500 mA and at 127°C for 360 mA. For both curves, the agreement between theory and experiment is very close.

Although the numerical solution is needed for accurate results, the diode behavior can be better understood from approximate relations. Therefore, assume $\omega_R^2/\omega^2 \ll 1$; this is not a bad approximation under the conditions of Figs. 5 and 6 and since ω_R^2 is fixed for fixed V_{rf} and I_{dc}, the approximation becomes better at higher frequencies. Then, we neglect terms proportional to ω_R^2/ω^2 in (A1), and obtain from the oscillation requirement of (2)

$$g = \frac{(1-\cos\theta)}{\theta} C_d \frac{\omega_R^2}{\omega} - \omega^2 C_d^2 R_s. \tag{11}$$

The power will drop as the frequency increases until $g = 0$ at the cutoff frequency

$$f_c = \frac{1}{2\pi}\left(\frac{(1-\cos\theta)}{\theta}\frac{\omega_R^2}{C_d R_s}\right)^{1/3}. \tag{12}$$

Near the cutoff frequency, $(1-\cos\theta)/\theta$ can generally be approximated as $2/\pi$ for values of R_s greater than 0.2 Ω.

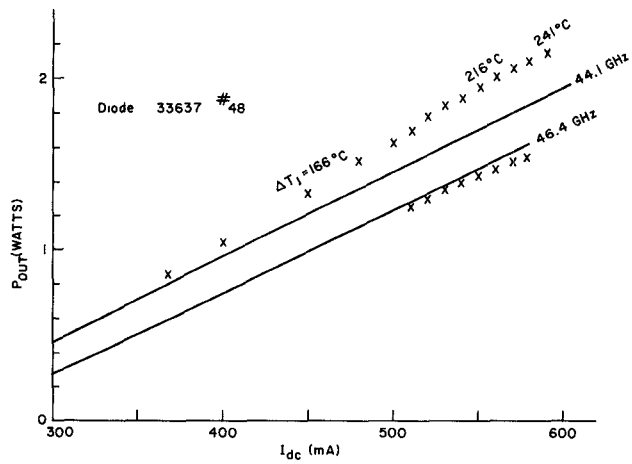

Fig. 9. Measured and calculated output power versus current for 44.1 and 46.4 GHz. The calculations assume $V_{\text{rfmax}} = 11$ V and $T = 200$°C. ΔT_j is listed for several experimental points.

Moreover, near cutoff, V_{rf} will approach zero so that ω_R^2 approaches the avalanche frequency ω_a^2. Thus, the cutoff frequency is proportional to the $1/3$ power of I/R_s and, for fixed current, the cutoff frequency is proportional to $A^{-2/3}$.

The analytical model allows us to calculate the effect of making specific changes in diode parameters. For example, Fig. 7 shows the effect of reducing R_s from the value of 0.39 Ω used in Fig. 6 to 0.3, 0.2, and 0.1 Ω. Since we are now able to produce diamond heat sinks with R_s less than 0.2 Ω, we should be able to obtain higher powers and wider bandwidth as indicated by the figure.

The effect of changing V_{rfmax} to 9 and 13 V from the original value of 11 V used in the earlier calculations is shown in Fig. 8. An increase in V_{rfmax} increases the output power at intermediate frequencies, but it does not increase the cutoff frequency since V_{rf} drops below V_{rfmax} and approaches zero as the cutoff frequency is approached.

The junction temperatures shown in Figs. 5 and 6 are nearly constant as a function of frequency, although it can be seen that they increase slightly as the RF output power drops so that more input power must be dissipated as heat. The values of ΔT_j, shown in Figs. 5 and 6, were based on the measured dissipated power using values of thermal resistance measured by a technique similar to that described by Haitz [10].

V. Measurements of Output Power Versus DC Current

Since the diode with the diamond heat sink was not thermally limited at 500 mA, one can choose a particular frequency and push the dc current higher. The output powers measured at 44.1 GHz and at 46.4 GHz are indicated by the crosses in Fig. 9, while the solid curves are calculated from the numerical model assuming $V_{\text{rfmax}} =$ 11 V and a temperature of 200°C.

As the current is increased, the output power increases in fairly good agreement with the calculated power. However, attempts to push the power level beyond 590 mA for the 44.1-GHz experiment led to a rapid drop in the output

power. At present it is not clear whether this is associated with a threshold for instability for subharmonic oscillations [11], [12], or whether we have reached the largest value of conductance achievable with the given operating frequency and diode capacitance.

The power output at 44.1 GHz reached a maximum of 2.15 W and 14.4-percent efficiency at 590 mA.

VI. Conclusions

Power output over a frequency band from 33–50 GHz has been demonstrated and shown to agree with the results calculated from an analytical model using experimentally demonstrated values for R_s and V_{rfmax}. In particular, it was not necessary to invoke the negative differential conductivity of n-GaAs, the RF motion of the depletion edge, nor drift region ionization in order to explain the high power results.

The power output of these diodes is dependent on V_{rfmax}, whose value has been measured experimentally but whose determination is imperfectly understood. Nevertheless, it seems plausible that the high mobility of electrons at low fields in GaAs and the appropriately designed lo–hi–lo Read or hybrid profile which avoids drift-region ionization while keeping carrier velocities saturated at moderate RF swings, have helped us to attain the relatively high values of V_{rf} which produced the good efficiency and power which we have measured in this study.

The experiments also showed that somewhat higher CW power could be obtained with improved heat sinking. However, even in the absence of a thermal limitation, the output power was limited because it saturated abruptly at a critical current. A similar situation occurred in X-band diodes when the thermal limitation was effectively removed by going to pulsed operation [3]. The achievement of even higher output power would become possible if circuits could be designed to increase this critical current or if V_{rfmax} could be increased. Improvements in technology, since the experiments described in this paper, have already resulted in diamond-packaged EHF diodes with thermal resistances less than 15°C/W and with series resistance on the order of 0.2 Ω or less. These improvements will allow some increase in output power without changing the doping profile or the external circuit.

Appendix
The Analytic Read Diode Model

The analytical model [1]–[4] expresses the admittance $Y = G + jB$ as

$$Y = \frac{j\omega C_d\left(1-\omega_R^2/\omega^2\right)}{1-\frac{\omega_R^2}{\omega^2}\left(\frac{w_n}{w_T}\left(1+F_n\right)+\frac{w_p}{w_T}\left(1+F_p\right)\right)} \tag{A1}$$

where the angular resonance frequency is

$$\omega_R^2 = h(b)\,\omega_a^2 \tag{A2}$$

where ω_a is the usual avalanche frequency

$$\omega_a^2 = \frac{3\alpha' v_s}{\epsilon} j_{\text{dc}} \tag{A3}$$

where j_{dc} is the current density, α' is the derivative of the ionization coefficient with respect to field, ϵ is the dielectric constant, and $v_s = 2v_n v_p/(v_n + v_p)$, where v_n and v_p are the saturated carrier velocities. The quantity b is a nondimensional form of the RF voltage

$$b = \frac{3\alpha' v_s}{\omega w_T \gamma} V_{\text{rf}} \tag{A4}$$

where γ, which is normally close to unity, is given by

$$\gamma^2 = \left[1-\frac{\omega_R^2}{\omega^2}\left(\frac{w_n}{w_T}\left(1-\frac{\sin\theta_n}{\theta_n}\right)+\frac{w_p}{w_T}\left(1-\frac{\sin\theta_p}{\theta_p}\right)\right)\right]^2 + \left[\frac{\omega_R^2}{\omega^2}\left(\frac{w_n}{w_T}\left(\frac{1-\cos\theta_n}{\theta_n}\right)+\frac{w_p}{w_T}\left(\frac{1-\cos\theta_p}{\theta_p}\right)\right)\right]^2. \tag{A5}$$

Also

$$F_n = \frac{e^{-j\theta_n}-1}{j\theta_n}$$

and $\theta_n = \omega w_n/v_n$ and similarly for F_p and θ_p. The diode capacitance $C_d = \epsilon A/w_T$ and w_T and $w_T = w_n + w_p$ is the total width of the diode.

Assuming that the saturation current is negligible, the function $h(b)$ in (A2) is

$$h(b) = \frac{2I_1(b)}{bI_0(b)}$$

where I_0 and I_1 are the modified Bessel functions of order 0 and 1.

Given b and j_{dc}, as well as the physical parameters of the diode. (A1)–(A5) can be solved explicitly to give Y and V_{rf}. The numerical solution, with V_{rf} and j_{dc} given, is obtained by iterating the calculation which converges rapidly to the correct values b and Y.

Acknowledgment

We thank G. Jerinic and D. Massé for their support, and we are indebted to members of the IMPATT diode group of the Raytheon Research Division's Semiconductor Laboratory for their contributions to the ideas and the technology of these devices and circuits.

References

[1] H. Statz, R. A. Pucel, J. E. Simpson, and H. A. Haus, "Noise in gallium arsenide avalanche Read diodes," *IEEE Trans. Electron Devices*, vol. ED-23, pp. 1075–1085, Sept. 1976.

[2] M. G. Adlerstein, J. W. McClymonds, and H. Statz, "Avalanche response time in GaAs as determined from microwave admittance measurements," *IEEE Trans. Electron Devices*, vol. ED-28, pp. 808–811, July 1981.

[3] L. H. Holway, Jr., M. G. Adlerstein, K. K. Johnson, B. Lauterwasser, D. Masse, J. W. McClymonds, S. R. Steele, and R. N. Wallace, "High power pulsed avalanche diodes," Raytheon Co. Final Rep. to U.S. Air Force Avionics Lab, Contract F33615-78-C-1499, Oct. 1980.

[4] M. G. Adlerstein and E. L. Moore, in *Proc. 8th Biennial Conf. Active Microwave Semiconductor Devices and Circuits*, Cornell Univ., 1981.

[5] M. G. Adlerstein, L. H. Holway, and S. L. Chu, "Measurement of series resistance in IMPATT diodes," submitted to *IEEE Trans. Electron Devices*.

[6] T. Misawa and N. D. Kenyon, "An oscillator circuit with cap structures for millimeter-wave IMPATT diodes," *IEEE Trans. Microwave Theory Tech.*, vol. MTT-18, pp. 969–970, Nov. 1970.
[7] W. T. Read, Jr., "A proposed high-frequency negative-resistance diode," *Bell System Tech. J.*, vol. 37, pp. 401–466, Mar. 1958.
[8] L. H. Holway, Jr., S. R. Steele, and M. G. Adlerstein, "Measurement of electron and hole properties in *p*-type GaAs," in *Proc. 7th Biennial Conf. Active Microwave Semiconductor Devices and Circuits*, Cornell Univ., pp. 199–208, 1979.
[9] P. A. Houston and A. G. R. Evans, "Electron drift velocity in *n*-GaAs at high electric fields," *Solid-State Electron.*, vol. 20, pp. 197–204, 1977.
[10] R. H. Haitz *et al.*, "A method for heat flow resistance measurements on avalanche diodes," *IEEE Trans. Electron Devices*, vol. ED-16, pp. 438–445, May 1963.
[11] M. G. Adlerstein, H. Statz, and J. McClymonds, private communication.
[12] J. Gonda and W. E. Schroeder, "IMPATT diode circuit design for parametric stability," *IEEE Trans. Microwave Theory Tech.* vol. MTT-24, pp. 343–352, May 1977.

✤

Lowell H. Holway, Jr. was born in St. Louis, MO., on October 7, 1931. He received the B.A. degree in mathematics from Dartmouth College, Hanover, NH, in 1953. After receiving the M.A. degree in physics from Harvard University, Cambridge, MA, in 1955, he joined the Raytheon Research Division where he initially was involved in studies in nuclear reactor physics. In 1959, he returned to Harvard University under the sponsorship of the Raytheon Graduate Program and received his Ph.D. degree in applied mathematics in 1964, with a thesis entitled, "Approximation Procedures in Kinetic Theory."

Subsequently, he returned to the Raytheon Research Division where he was involved as a Principal Research Scientist in a number of programs such as the generation of magnetic instability in the ionospheric plasma by high power HF transmissions and the avalanche breakdown of insulating crystals by high-power laser radiation. Since 1974, he has been involved with modeling the device physics of IMPATT diodes and with measurements of the properties of GaAs. He has supervised measurements of trap lifetimes in GaAs by DLTS techniques, measurements of ionization coefficients and hole velocity in GaAs, and PITS measurements of trap activity in highly-resistive GaAs. While at Raytheon, he has been author or coauthor of 32 publications in books or journals and has given 22 talks at meetings and symposia.

Dr. Holway is a member of the American Physical Society and Phi Beta Kappa.

✤

Shiou Lung Chu was born in London, England. She received the B.S. degree in physics from Fu-Jen University in Taipei, Taiwan, in 1971 and the M.A. degree, also in physics, from Boston University in Boston, MA, in 1973.

She joined the Raytheon Research Division, Lexington, MA, in 1973. She has worked on silicon TRAPATT and Gunn devices, GaAs IMPATT oscillators, and combiners. Since 1978 she has been engaged in the research and development of millimeter-wave GaAs IMPATT diodes and circuits. She is a Senior Scientist and is currently working on pulsed IMPATT diodes.

A Multiple-Device Cavity Oscillator Using Both Magnetic and Electric Coupling Mechanisms

MOHAMMAD MADIHIAN, STUDENT MEMBER, IEEE, ANDREZEJ MATERKA, AND SHIZUO MIZUSHINA, MEMBER, IEEE

Abstract—**This paper presents a novel concept to increase the number of active devices combined in a cavity oscillator by coupling them to both electric and magnetic fields inside the cavity. The structure employs probes and coaxial lines for electric and magnetic coupling, respectively. The sum of the output powers from individual devices combined can be obtained by properly adjusting the coupling factors of the circuit. Operation principles of the circuit are analyzed for probe coupling, and results are applied to explain the operation of the circuit when both probe and coaxial coupling are used. The circuits described here are free from moding instabilities. Prototype circuits have been constructed at *X*-band, using Gunn diodes, for experimental confirmation of the theory developed.**

Manuscript received April 30, 1982; revised July 7, 1982.

M. Madihian and S. Mizushina are with the Research Institute of Electronics, Shizuoka University, Hamamatsu 432, Japan.

A. Materka was with the Research Institute of Electronics, Shizuoka University, Hamamatsu 432, Japan. He is now with the Institute of Electronics, Lodz Technical University, ul. Gdanska 176, Lodz, Poland.

I. INTRODUCTION

THE SINGLE-TUNED oscillators invented by Kurokawa *et al.* [1] and Harp *et al.* [2] have received considerable development and application as the most successful power combining techniques at microwave and millimeter-wave frequencies [3]–[7]. Nevertheless, the increasing need for higher and higher output power may

0018-9480/82/1100-1939$00.75 ©1982 IEEE